This is a preprint, the final version is subject to change, of the American Mineralogist (MSA)
Cite as Authors (Year) Title. American Mineralogist, in press.
(DOI will not work until issue is live.) DOI: http://dx.doi.org/10.2138/am-2016-5394

Revision_2

Phase transitions between high- and low-temperature orthopyroxene in the $Mg_2Si_2O_6$-$Fe_2Si_2O_6$ system

Shugo Ohi[1,2] and Akira Miyake[2]

[1] Faculty of Education, Shiga University, Otsu 520-0862, Japan (s-ohi@edu.shiga-u.ac.jp)

[2] Graduate School of Science, Kyoto University, Kyoto 606-8502, Japan

Abstract

We observed isosymmetric phase transitions of orthopyroxene in the $Mg_2Si_2O_6$-$Fe_2Si_2O_6$ system during high-temperature in situ X-ray powder diffraction experiments with a multiple-detector system and a high-temperature strip heater chamber in an atmosphere of Ar plus 1% H_2. The transition temperatures we determined for natural orthopyroxenes were 1113–1147, 1120–1139, and around 1200 °C for Fs_{10}, Fs_{14}, and Fs_{37}, respectively, and those for synthetic orthopyroxenes were 1048–1075, 961–1048, and 1037–1148 °C for Fs_{20}, Fs_{30}, and Fs_{46}, respectively. Our experiments showed that the transition from low- to high-temperature orthopyroxene in the $Mg_2Si_2O_6$-$Fe_2Si_2O_6$ system occurred at about 1000–1200 °C. We concluded that the stability field of low-temperature orthopyroxene was below 1000 °C and that of high-temperature orthopyroxene was above 1200 °C.

Keywords: orthopyroxene, X-ray powder diffraction, isosymmetric phase transition, enstatite-ferrosilite system

Introduction

Pyroxene is an important rock-forming mineral because of its abundance in the Earth's crust, its paragenetic association with ore minerals, and the information it can provide on the thermal history of pyroxene-bearing rocks. The composition of most natural pyroxene lies within the $Mg_2Si_2O_6$-$CaMgSi_2O_6$-$CaFeSi_2O_6$-$Fe_2Si_2O_6$ (En-Di-Hd-Fs) system. The phase relationships established within the En-Di-Hd-Fs system in many studies (see Huebner and Turnock 1980, p. 227) show four stable pyroxene phases: orthopyroxene (Opx, space group *Pbca*), protopyroxene (Ppx, space group *Pbcn*), pigeonite (Pig, space group $C2/c$ at high temperature and $P2_1/c$ at low temperature), and augite (Aug, space group $C2/c$).

Polymorphs of $Mg_2Si_2O_6$ pyroxene have been identified: low-temperature orthopyroxene (LT-Opx, space group *Pbca*), low-temperature clinopyroxene (LT-Cpx, space group $P2_1/c$), Ppx, high-temperature orthopyroxene (HT-Opx, space group *Pbca*), high-temperature clinopyroxene (HT-Cpx, space group $C2/c$), and high-pressure clinopyroxene (HP-Cpx, space group $C2/c$). Ppx, HT-Opx, HT-Cpx, and HP-Cpx are unquenchable phases; Ppx, HT-Cpx, and HP-Cpx invert to LT-Cpx during quenching; and HT-Opx inverts to LT-Opx during quenching. LT-Cpx is the same crystal structure as Pig at low temperature and HT-Cpx is the same crystal structure as Pig at high temperature and Aug.

High-pressure phases other than HP-Cpx have been reported: Yang et al. (1999) reported high-pressure $P2_1cn$ pyroxene, Zhang et al. (2012) and Finkelstein et al. (2015) reported high-pressure $P2_1/c$ pyroxene, and Finkelstein et al. (2015) reported two types of high-pressure $Pca2_1$ pyroxene.

Opx, Ppx, and Pig are Ca-poor pyroxenes with stability fields near the En-Fs system. In the phase diagram of the En-Fs system of Bowen and Schairer (1935), Opx is a low-temperature phase and Pig (described by them as clinopyroxene) is a high-temperature phase. However, Atlas (1952) and Foster (1951) indicated that the stability field for Ppx is above 985 °C in a Ca-poor and Fe-free system. Furthermore, Huebner and Turnock (1980) proposed a stability field for Opx at high temperature on the basis of synthetic experiments. Huebner (1980) researched phase relationships in the En-Fs system and reconstructed the phase diagram for the system (Fig. 1).

There has been controversy about the existence and stability within the En-Di system of a Ca-bearing Opx phase (other than Ppx) identified by Foster and Lin (1975) near 1400 °C. At room temperature, the Ca-bearing Opx gave the same diffraction pattern as Ca-free Opx that was stable below 1000 °C. However, the schematic P-T projection of binary univariant equilibria required strong curvature along the Opx = Ppx + Di and Ppx + Pig = Opx reactions if Ca-bearing Opx near 1400 °C was to be equivalent to Ca-free Opx below 1000 °C. Carlson (1985, 1988) proposed that the Ca-bearing Opx is a different phase from Ca-free Opx, but provided no supporting evidence

(Carlson et al. 1988).

The existence of a high-temperature orthorhombic phase, different from LT-Opx, was suggested by Ohashi and Finger (1973) and Pannhorst (1979). After the discovery of natural Pig with space group $P2_1/c$ (Morimoto 1956), Morimoto and Koto (1969) showed that the orthorhombic cell is composed of two monoclinic $P2_1/c$ pyroxene cells. The transition of monoclinic pyroxene between $P2_1/c$ and $C2/c$ with increasing temperature was suggested by Morimoto and Tokonami (1969) and confirmed by Smith (1969). In this transition, two different silicate chains in $P2_1/c$ are stretched and changed to one type in $C2/c$ and one M2-O3B_1 bond alters another M2-O3B_2 bond. Ohashi and Finger (1973) suggested the existence of a new HT-Opx phase with the same space group as LT-Opx (*Pbca*) and composed of two monoclinic $C2/c$ pyroxene cells. Pannhorst (1979) suggested a similar crystal structure, composed of stretched silicate chains and an M2-O3B_2 bond that differs from the M2-O3B_1 of LT-Opx.

In a high-temperature in situ X-ray study of $(Mg_{0.75}Fe_{0.25})_2Si_2O_6$ synthetic Opx, at 1027 °C Yang and Ghose (1995) observed two crystallographically distinct stretched silicate chains and a new M2-O3B_2 bond in the structure. However, they could not identify a discontinuous change between LT-Opx and HT-Opx, which was a requirement for isosymmetric structural change of a first-order phase transition (Christy 1995), and they suggested that $(Mg_{0.75}Fe_{0.25})_2Si_2O_6$ Opx at 1027 °C is a transitional structural state between Opx and Ppx. Subsequently, Miyake et al. (2004) observed a discontinuous isosymmetric phase transition between LT-Opx and HT-Opx in a molecular dynamics simulation. The HT-Opx they identified showed almost the same crystal structure as that of Yang and Ghose (1995).

More recently, Ohi et al. (2008) observed double peaks of Opx at 1170 °C in high-temperature X-ray powder diffraction (HT-XRD) experiments and proved that the transition between LT-Opx and HT-Opx is a discontinuous isosymmetric phase transition. Ohi et al. (2008, 2010) concluded that there are two different Opx phases, LT-Opx and HT-Opx, and that the Ca-bearing Opx phase near 1400 °C in the En-Di system is HT-Opx. The HT-Opx had not previously been observed in investigations of the En-Di phase system because it is an unquenchable phase and has the same space group as LT-Opx.

Before the discovery of the HT-Opx stability field in the En-Di system, the En-Di-Hd-Fs system was drawn without taking into account the existence of both LT-Opx and HT-Opx. As shown in Figure 1, the stability field of Opx extends to about 1400 °C. The purpose of this study is to use HT-XRD to observe the transition from Fe-bearing LT-Opx to HT-Opx and to distinguish the LT-Opx and HT-Opx stability fields within the En-Fs system.

Method

Sample preparation

The starting materials for HT-XRD were natural samples of Fs_{10}, Fs_{14}, and Fs_{37} (hereafter, $Fs_{10}N$, $Fs_{14}N$, and $Fs_{37}N$) and synthetic samples of Fs_{20}, Fs_{30}, and Fs_{46} (hereafter, $Fs_{20}S$, $Fs_{30}S$, and $Fs_{46}S$). These were examined by XRD (Rigaku SmartLab), optical microscope, and scanning electron microscope (HITACHI S-3000) with energy dispersive X-ray (HORIBA EMAX7000). Chemical analyses of Opx in all samples and source locations for natural Opx samples are given in Table 1.

Crystals of synthetic samples were synthesized from gels that were prepared from Mg metal, $Fe(C_2O_4)2H_2O$, and tetraethyl orthosilicate. A gel pellet of bulk composition $MgO:FeO:SiO_2$ = 0.79:0.21:1.08 (mol ratio) was prepared for $Fs_{20}S$. The pellet was placed in SiO_2 (cristobalite) powder in a Pt crucible to prevent Fe in the gel alloying with Pt during heating (Fig. 2). The pellet was heated in a one-atmosphere gas mixing (H_2-CO_2) furnace at 1415 °C for 3 days. The furnace oxygen fugacity was maintained near that of an iron-wüstite buffer. The recovered charge consisted of Opx, SiO_2 (cristobalite), and glass.

$Fs_{30}S$ was synthesized from a gel of bulk composition $MgO:FeO:SiO_2$ = 0.68:0.32:1.09 (mol ratio). The gel was loaded into a Pt capsule surrounded by a Ni-NiO capsule and placed in a Boyd-England type piston-cylinder apparatus at 1350 °C and 1GPa for 2 h. The recovered charge consisted of Opx and a small amount of magnetite (Mgt).

$Fs_{46}S$ was synthesized from a gel of bulk composition $MgO:FeO:SiO_2$ = 0.45:0.55:1.10 (mol ratio) at 1230 °C and 1GPa for 3 h by same method as used for $Fs_{30}S$. The recovered charge consisted of Opx and Mgt. The weights of $Fs_{30}S$ and $Fs_{46}S$ were about 10 mg and their diffraction intensities were lower than those of the other samples.

The natural and synthetic Opx samples were ground before HT-XRD analysis.

High temperature X-ray diffraction

HT-XRD experiments were done by using the multiple-detector system used by Toraya et al. (1996) with a high-temperature strip heater chamber (HTK 16N; Anton Paar GmbH) at the BL-4B2 beam line at the Photon Factory of the High Energy Accelerator Research Organization in Tsukuba, Japan. The counting loss of the detection system was corrected by the method of Ida (2008). The peak wavelength of the source X-ray beam was determined by analysis of diffraction peak profiles (Ida et al. 2003) of a standard Si powder (NIST SRM640c). The observed diffraction intensities were corrected for the effect of intensity enhancement in asymmetric diffraction (Toraya

et al. 1993). An AlN sample holder (0.5 × 10 × 20 mm plate; FAN-170 grade) was used because of its high heat conductivity and was heated by a Pt plate filament (1 × 10 ×100 mm).

The temperature of the furnace was controlled by an S-type (Pt/Pt-10 wt% Rh) thermocouple welded just below the center of the Pt filament. Sample temperatures were calibrated according to the α–β quartz transition temperature (573 °C) and the low- to high-temperature orthoenstatite transition temperature (1120 °C). Diffraction peaks of both α and β quartz were observed at temperatures over 50 °C during calibration experiments, although this phase transition occurred rapidly. Diffraction peaks of both low- and high-temperature orthoenstatite were observed at temperatures over 70 °C. These observations indicate large differences between the highest and lowest temperatures within the samples (~50 °C at 573 °C and ~70 °C at 1120 °C). In this study, the temperature at which β quartz (high-temperature orthoenstatite) began to appear was taken to be 573 °C (1120 °C). Hence, the temperatures in our study reflect those of the hottest parts of the samples.

An atmosphere of Ar plus 1% H_2 was passed through the chamber during heating to prevent oxidation of Fe. The wavelengths of X-ray beams used were 1.19729(1) Å for natural Opx (Fs_{10} and Fs_{37}), 1.19719(1) Å for natural Opx (Fs_{14}), and 1.19619(3) Å for synthetic Opx (Fs_{20} and Fs_{30}). The scanning step interval was 0.01° and the diffraction angle (2θ) ranged from 8.00 to 155.00°. Unit cell dimensions (Table 2) were determined by least-squares fitting by using the PDIndexer software produced by Y. Seto (Kobe University; http://www2.kobe-u.ac.jp/~seto/).

Results

$Fs_{10}N$ and $Fs_{14}N$

The peak profiles of $Fs_{10}N$ and $Fs_{14}N$ (Fig. 3a to d) show that the only crystalline phases during the HT-XRD experiments were Opx and the samples recovered after the experiments also consisted entirely of Opx. The diffraction patterns of LT-Opx in $Fs_{10}N$ did not change markedly below 1113 °C, whereas new diffraction peaks appeared near those of LT-Opx above 1147 °C (Fig. 3a and b). They do not represent LT-Cpx, HT-Cpx, HP-Cpx, high-pressure $P2_1/c$, $P2_1cn$ pyroxene, or Ppx because (1) no new peaks separate from those of LT-Opx were observed, (2) new peaks appeared near $h = odd$, and (3) the recovered samples consisted entirely of LT-Opx. The diffraction patterns resemble those of LT-Opx, and all of the new peaks could be indexed to an orthorhombic cell with similar lattice constants to LT-Opx. However, most of the new peaks were at lower values of 2θ than those of LT-Opx (as observed also by Ohi et al. 2008), whereas the unit cell volume of $Pca2_1$ pyroxene might be smaller than that of LT-Opx. The new peaks we observed were indexed as planes of HT-Opx. The phase that appeared above 1147 °C was considered to be HT-Opx and crystal structure of HT-Opx was same as that of $(Mg_{0.75}Fe_{0.25})_2Si_2O_6$ synthetic Opx at 1027 °C by Yang and Ghose (1995). Ohi et al. (2008) showed that the thermodynamic behavior of HT-Opx differs from that of low-temperature orthoenstatite because LT-Opx of $Ca_{0.06}Mg_{1.94}Si_2O_6$ composition is equivalent to low-temperature orthoenstatite, but with a slightly larger M2 site (Nestola and Tribaudino 2003).

Therefore, an isosymmetric phase transition from LT-Opx to HT-Opx occurred between 1113 and 1147 °C. Hysteresis of this transition might be small and the transition temperature of natural Opx in $Fs_{10}N$ was slightly lower than 1113–1147 °C. Ohi et al. (2008) reported that hysteresis of the transition of LT-Opx of $Ca_{0.06}Mg_{1.94}Si_2O_6$ composition was too low to be observed in experiments conducted at temperature intervals of 10 °C.

In the transition from LT-Opx to HT-Opx, the *a* and *c* dimensions and volume increased abruptly, whereas the *b* dimension decreased (Fig. 4a). HT-Opx was an unquenchable phase that inverted to LT-Opx during quenching so that the recovered samples consisted entirely of LT-Opx.

Our HT-XRD experiments for $Fs_{14}N$ showed a similar transition from LT-Opx to HT-Opx between 1120 and1139 °C (Figs. 3c, 3d, and 4b).

$Fs_{37}N$

The peak profiles of $Fs_{37}N$ (Fig. 3e and f) show that the only crystalline phases below 1079 °C were Opx. Diffraction patterns of olivine (Ol) appeared above 1147 °C and new peaks (d = 3.357 and 3.088 Å) that did not represent LT-Opx, Ol, iron oxide, SiO_2, or Ppx appeared at 1196 °C (Fig. 3e). Jiang et al. (2002) reported that LT-Cpx of $Mg_2Si_2O_6$ composition at 1100 °C showed a strong *d*

182 = 3.32 Å peak, which is close to and may explain the d = 3.357 Å peak of our study, but the d =
183 3.088 Å peak we observed could not be indexed as a plane of LT-Cpx. In a high-temperature X-ray
184 study of enstatite, Jiang et al. (2002) similarly observed two extra peaks at 1200 °C, at d =
185 3.075–3.079 Å and 3.323–3.331 Å. HT-Cpx reported by Smith (1969) had the strongest peak for the
186 HT-Cpx $22\bar{1}$ reflection (d = 3.06 Å), and a strong peak for the HT-Cpx 021 reflection (d = 3.34 Å);
187 Jiang et al. (2002) concluded that these peaks originate from HT-Cpx. HT-Cpx of $(Mg_{0.7}Fe_{0.3})_2Si_2O_6$
188 composition at 900 °C reported by Smyth (1972) had the strongest peak at d = 3.08Å, a strong peak
189 at d = 3.36Å, and two new peaks at 1196 °C that could be indexed to HT-Cpx 021 and HT-Cpx $22\bar{1}$.
190 Other strong HT-Cpx reflections, such as those of 220 and 310, might overlap the LT-Opx 420 and
191 610 reflections, respectively. At 1269 °C, the intensities of Opx diffraction peaks for $Fs_{37}N$ were
192 markedly lower and exhibited tails on the high-2θ side (Fig. 3e and f).
193 Below 1196 °C, the unit cell dimensions and volumes of Opx in $Fs_{37}N$ increased with
194 increasing temperature, but between 1196 and 1269 °C they decreased (Fig. 4c). The sample
195 recovered after the HT-XRD experiments showed that $Fs_{37}N$ partially melted at high temperature,
196 indicating that the presence of minor elements such as Al, Ca, and Mn decreased the solidus
197 temperature of Opx, that Fe content in Opx declined during the Opx → Ol + liquid reaction
198 between 1196 and 1269 °C, and that the unit cell dimensions and volumes of Opx at 1269 °C
199 declined to values smaller than those at 1196 °C.
200 The unit cell volumes of Opx did not show discontinuous change below 1196 °C, but the
201 volume thermal expansion coefficients increased at around 1000 °C (Fig. 4c). Ohi et al. (2008)
202 reported similar increases of volume thermal expansion coefficients before the transition from
203 LT-Opx to HT-Opx. This increase of volume thermal expansion coefficients of Opx ($Fs_{37}N$)
204 indicates that the LT-Opx to HT-Opx transition occurred between 1147 and 1196 °C or above 1200
205 °C.
206
207 **$Fs_{20}S$ and $Fs_{30}S$**
208 The peak profiles of $Fs_{20}S$ and $Fs_{30}S$ (Fig. 3g to j) show that the crystalline phases during
209 our HT-XRD experiments were Opx. As was the case for $Fs_{10}N$ and $Fs_{14}N$, the transition from
210 LT-Opx to HT-Opx in $Fs_{20}S$ occurred between 1048 and 1075 °C (Figs. 3g and h and 4d) and that
211 for $Fs_{30}S$ occurred between 961 and 1048 °C (Figs. 3i and j and 4e). The samples of $Fs_{20}S$ and $Fs_{30}S$
212 recovered after the HT-XRD experiments consisted entirely of LT-Opx.
213
214 **$Fs_{46}S$**
215 The peak profiles of $Fs_{46}S$ (Fig. 3k and l) show that the crystalline phases were Opx + Mgt

at 721 and 802 °C. Diffraction patterns of Ol began to appear at 882–960 °C, those of quartz (Qtz) appeared at 999–1037 °C, and the Mgt peaks disappeared at 960–999 °C. The peak profiles indicate that the Opx + Mgt = Ol reaction occurred between 882 and 960 °C during our experiments and the Opx = Ol + Qtz reaction occurred above 999 °C; these temperatures are within the stability field of Opx of $(Mg_{54}Fe_{46})_2Si_2O_6$ composition (Fig. 1). The composition of Opx in $Fs_{46}S$ changed during these reactions, although the change was minor because the change of unit cell dimensions and volumes was linear below 1037 °C (Fig. 4f). All of the peaks at 1037 and 1148 °C represent Ol, Qtz, or Opx and the unit cell dimensions and volumes showed discontinuous change between 1037 and 1148 °C; hence, the transition from LT-Opx to HT-Opx in $Fs_{46}S$ occurred between those temperatures (Fig. 4f).

Discussion

Relationship of transition temperature and Fe content of Opx

Ohi et al. (2010) showed that the transition from LT-Opx ($Mg_2Si_2O_6$) to HT-Opx occurred between 1108 and 1129 °C. In our study, the temperatures of the transition from synthetic LT-Opx to HT-Opx in $Fs_{20}S$ and $Fs_{30}S$ were lower than that for $Mg_2Si_2O_6$ Opx. High-temperature in situ single-crystal X-ray diffraction experiments by Yang and Ghose (1995) showed that the unit cell volumes of synthetic Opx of $(Mg_{0.75}Fe_{0.25})_2Si_2O_6$ composition increased sharply between 927 and 1027 °C. The structure of Opx at 1027 °C according to Yang and Ghose (1995) was almost the same as the high-temperature phase of orthoenstatite simulated by Miyake et al. (2004). Yang and Ghose (1995) showed that the transition from synthetic $(Mg_{0.75}Fe_{0.25})_2Si_2O_6$ LT-Opx to HT-Opx occurred at 927–1027 °C. Thus, the results of our HT-XRD experiments for Opx in $Fs_{20}S$ and $Fs_{30}S$ were consistent with those of Yang and Ghose (1995). In our experiments, the temperature at which the phase transition of synthetic $(Mg_{1-0.7}Fe_{0-0.3})_2Si_2O_6$ Opx occurred decreased with increasing Fe content, but the transition temperature for $Fs_{46}S$ was higher than that for $Fs_{30}S$. In the experiments of Yang and Ghose (1994), synthetic Opx of $(Mg_{0.61}Fe_{0.39})_2Si_2O_6$ and $(Mg_{0.49}Fe_{0.51})_2Si_2O_6$ compositions underwent continuous compositional change between 727 and 1027 °C; for synthetic Opx of $(Mg_{0.25}Fe_{0.75})_2Si_2O_6$ and $(Mg_{0.17}Fe_{0.83})_2Si_2O_6$ composition these changes occurred between 727 and 927 °C. Yang and Ghose (1994) did not observe a transition from LT-Opx to HT-Opx. Therefore, the transition temperature of Opx of Fe content richer than $(Mg_{0.61}Fe_{0.39})_2Si_2O_6$ might be higher than 1027 °C. In our study, the phase transition of Opx in $Fs_{46}S$ was observed above 1027 °C. The temperature at which the phase transition for synthetic $(Mg_{0.7-0.5}Fe_{0.3-0.5})_2Si_2O_6$ Opx occurred increased with increasing Fe content. Thus, the results of our HT-XRD experiments on Opx in $Fs_{46}S$ were consistent with those of Yang and Ghose (1994).

On the other hand, our results showed that phase transitions from LT-Opx to HT-Opx for natural Opx occurred at higher temperatures than those for synthetic Opx. The transition temperatures for Opx in $Fs_{10}N$ and $Fs_{14}N$ were almost the same as that reported by Ohi et al. (2010) for Opx of $Mg_2Si_2O_6$ composition, but the transition temperature we observed for natural Opx in $Fs_{37}N$ was higher than that reported by Ohi et al. (2010) for $Mg_2Si_2O_6$. Our experiments showed that the temperature of the phase transition for natural $(Mg_{0.8-0.6}Fe_{0.2-0.4})_2Si_2O_6$ Opx increased with increasing Fe content.

The above difference of the transition temperatures for natural and synthetic Opx might be related to the minor elements present in natural Opx, such as Na, Al, Ca, and Mn. Arlt et al. (2000) reported that for clinopyroxene, the temperature for the phase transition from $P2_1/c$ to HT-$C2/c$ was

influenced by the presence of Na, Al, Ca, and Mn. HT-XRD experiments by Ohi et al. (2008, 2010) showed that the transition temperature for Opx is also influenced by Ca content. Other elements (e.g., Na, Al, and Mn) would also influence the transition temperature of Opx. The results of our HT-XRD experiments on natural Opx are inconsistent with those of high-temperature, in situ neutron powder diffraction experiments by Gatta et al. (2007) on natural Opx derived from a xenolith; they did not identify a transition from LT-Opx to HT-Opx over a temperature range of 1200 to 150 °C. The discrepancy between our results and those of Gatta et al. (2007) may reflect the effect of small amounts of Al inserted into the T sites under high pressure in their sample.

Nonetheless, we observed the transition from LT-Opx to HT-Opx between 1000 and 1200 °C. Bowen and Schairer (1935) observed phase transitions from LT-Opx to Pig and from HT-Opx to Ppx. Opx synthesized by Huebner and Turnock (1980) near 1400 °C crystallized as HT-Opx and changed to LT-Opx during quenching. Huebner (1980) proposed a different phase diagram from that of Bowen and Schairer (1935) on the basis of synthetic experiments by Huebner and Turnock (1980). However, our results indicate that the Opx discussed by Bowen and Schairer (1935) was a different phase from that of Huebner and Turnock (1980). These experimental results are not contradictory; it is possible to construct a phase diagram for the En-Fs system that reflects the results of both Bowen and Schairer (1935) and Huebner and Turnock (1980).

Phase diagrams for the En-Fs system

Bowen and Schairer (1935) proposed a phase boundary between Opx and Pig according to their observation of phase transitions from Opx to Pig. The boundary was above the temperature at which the phase transition from LT-Opx of $(Mg_{0.8}Fe_{0.2})_2Si_2O_6$ composition to HT-Opx was observed. In this case, HT-Opx had separate stability fields around 1100 °C and 1400 °C and the thermochemical properties of the HT-Opx were inconsiderable. Hence, the phase boundary between LT-Opx and Pig was below the temperature of transition between LT-Opx and HT-Opx. The stability field of Opx was also below this temperature.

On the other hand, the stability field of Pig must be above the temperature of coexistence of Opx, Pig, and Aug in the En-Di-Hd-Fs systems proposed by Lindsley (1983), Turnock and Lindsley (1981), and Lindsley and Anderson (1983). In synthetic experiments at pressures of less than 1 atm in a Ca-bearing system, Turnock and Lindsley (1981) and Lindsley and Anderson (1983) showed that the coexistence temperature of these three phases was 1000 °C for chemical compositions of Mg : Fe = 50–60 : 50–40, and 1100 °C for Mg : Fe = 70–80 : 30–20. The reactions of Pig = Opx + Aug occurred at coexistence temperatures that were close to the lower limit of the stability fields of Pig in the $(Mg, Fe)_2Si_2O_6$-$Ca(Mg, Fe)Si_2O_6$ system. Hence, there was no stability field below

297 1000 °C for Pig of $(Mg_{0.5\text{-}0.6}Fe_{0.5\text{-}0.4})_2Si_2O_6$ composition in the En-Fs system or below 1100 °C for
298 Pig of $(Mg_{0.7\text{-}0.8}Fe_{0.3\text{-}0.2})_2Si_2O_6$ composition.
299 The experimental results of Turnock and Lindsley (1981), Lindsley and Anderson (1983),
300 and our results indicate that neither LT-Opx nor Pig have a stability field around 1100 °C and
301 composition $(Mg_{0.8}Fe_{0.2})_2Si_2O_6$. These studies show that phase relationships in this part of the phase
302 diagram are very complex because it lies close to the region of metastable coexistence of LT-Opx +
303 HT-Opx and LT-Opx + Pig, and the Gibbs free energies of these three phases are very similar.
304 Consistent stable phase assemblages around this area were for Pig + Ppx, a single phase of HT-Opx,
305 HT-Opx + Ppx, and HT-Opx + Pig. Experiments by Bowen and Schairer (1935) on natural Opx
306 samples of composition around $(Mg_{0.83}Fe_{0.17})_2Si_2O_6$ might well indicate the coexistence of Pig +
307 Ppx. In their experiments, natural $(Mg_{0.83}Fe_{0.17})_2Si_2O_6$ Opx samples did not change to other phases
308 without NaF, even at temperatures up to 1400 °C, whereas other Opx samples changed to Ppx or
309 Pig below 1100 °C. The sample of $(Mg_{0.83}Fe_{0.17})_2Si_2O_6$ composition Opx changed to Ppx or Pig at
310 1120 °C in their experiments with NaF. If the Gibbs free energies of Ppx and Pig of
311 $(Mg_{0.83}Fe_{0.17})_2Si_2O_6$ composition were higher than that of the single-phase Opx, $(Mg_{0.83}Fe_{0.17})_2Si_2O_6$
312 Opx in the region of coexistence of Ppx + Pig could not change to Ppx or Pig without element
313 diffusion. The Gibbs free energies of Pig and Opx were similar in this region of the phase diagram
314 and the diffusion and this reaction occurred slowly. In experiments with NaF, flux might well have
315 assisted the reaction of Opx → Ppx + Pig and both Ppx and Pig changed to $P2_1/c$ Cpx, but with
316 different chemical compositions.
317 Observations by Bowen and Schairer (1935) of Cpx inverted from $(Mg_{0.83}Fe_{0.17})_2Si_2O_6$ Opx
318 were possibly the result of insertion of Na into pyroxenes. In this case, the stability field of HT-Opx
319 would range from 1400 to 1100 °C.
320 The hypothetical phase diagram we developed in this study (Fig. 5) is a revision of that of
321 Huebner (1980) taking into account our results and those of past experiments on natural Opx and
322 Ca-bearing Opx (Bowen and Schairer 1935; Huebner and Turnock 1980; Lindsley and Anderson
323 1983).
324 Phase relationships near En-Fs system could change drastically with minor elements like
325 relationships near 1400 °C in the En-Di system. Phase relationships around 1100 °C and
326 $(Mg_{0.8}Fe_{0.2})_2Si_2O_6$ composition might also change with the addition of minor elements, because the
327 Gibbs free energies of LT-Opx, HT-Opx, and Pig are similar.
328 There have been few experiments examining phase relationships around 1100 °C and
329 $(Mg_{0.8}Fe_{0.2})_2Si_2O_6$ composition, where phase relationships might be very complex. In cases of
330 observations of natural samples, pyroxenes crystalized in this area might tend to form complex
331 structures. Further experiments are needed to clarify this area of the phase diagram for the En-Fs

system.

Appearance of Ol, HT-Cpx, and Qtz in $Fs_{37}N$ at 1196 °C and in $Fs_{46}S$ above 882 °C

During our HT-XRD experiments on $Fs_{46}S$, Ol and Qtz appeared at temperatures above 882 °C. The previous phase diagram for the En-Fs system (Fig. 1) indicates that the Opx → Ol + Qtz reaction occurs within a compositional range richer in Fe than Opx of Fs_{46} composition, which suggests that there may have been local compositional heterogeneity caused by Opx + Mgt → Ol reaction, and the reaction of Opx → Ol + Qtz occurred.

During our HT-XRD experiments for $Fs_{37}N$, diffraction patterns of Ol were observed without the appearance of Qtz. As with the case at 1269 °C, Ol at 1147 and 1196 °C might be the result of the Opx → Ol + liquid reaction. Because of the presence of Al, Ca, and Mn, the solidus temperature of natural Opx was lower than that of synthetic Opx, and Opx in $Fs_{37}N$ partially melted. The decrease of Fe content as a result of melting was too small at 1147 and 1196 °C and the unit cell dimensions and volumes of Opx below 1196 °C increased with increasing temperature. Diffraction patterns of HT-Cpx were also observed at 1196 °C, within the stability field of Opx of Fs_{37} composition in the phase diagram of Figure 1 and within the stability field of Pig (HT-Cpx) as shown in our revised phase diagram (Fig. 5). Thus, our study showed that Opx partially inverted to HT-Cpx during our high-temperature experiments.

Implications

Our results showed that transitions from LT-Opx to HT-Opx occurred in the En-Fs system between 1000 and 1200 °C and identified a stability field for HT-Opx that is not shown in the En-Fs system phase diagram of Huebner (1980), which is presently widely accepted. Thus, the results of our study suggest that the phase diagram for the En-Fs system needs to be revised.

Our experimental observations suggest that HT-Opx crystals may be common in the En-Fs system at low pressures and high temperatures in Fe^{2+}-bearing samples such as ordinary chondrites. For example, Tsuchiyama et al. (1988) observed heterogeneous textures in Opx in an ordinary type 3–4 chondrite. They interpreted the textures to represent an intermediate state in the metamorphic progression between petrologic types 3 and 4 ordinary chondrites. However, two Opx phases with different chemical compositions can coexist in equilibrium because the transition between LT-Opx and HT-Opx is a first-order transition. The heterogeneous textures of Opx noted by Tsuchiyama et al. (1988) might indicate the coexistence of LT-Opx and HT-Opx at around 1000–1200 °C. Microtextures, which are currently understood to represent an intermediate state, can be interpreted as the coexistence of LT-Opx and HT-Opx in equilibrium by using the new phase diagram, or a result of clustering of atoms in M sites before exsolution, as described by Tribaudino and Nestola (2002) and Tribaudino et al. (2002). Yanai and Kojima (1995) also observed two coexisting Opx phases with different chemical compositions that might also indicate the coexistence of LT-Opx and HT-Opx.

Yanai and Kojima (1995) considered Opx grains in the En-Di system in terms of CaO content and showed that at atmospheric pressure there is no stability field for Ca-free HT-Opx, whereas Ohi et al. (2010) showed that there is a stability field at around 1400 °C for Opx grains of $(Ca_{0.03\text{-}0.07}Mg_{1.97\text{-}1.93})Si_2O_6$ composition. Similarly, our study suggests that a stability field for HT-Opx exists in the En-Di-Hd-Fs system and that phase relationships in the system need to be remodeled, especially for the compositional range $(Ca_{0\text{-}0.1}Mg_{1\text{-}0.4}Fe_{0\text{-}0.5})Si_2O_6$ at temperatures above 1000 °C. Thus, the pyroxene thermometer at temperatures above 1000 °C and at atmospheric pressure needs to be re-examined. Further experiments for the Ca-bearing system are needed to improve the phase diagram for the En-Di-Hd-Fs system.

Acknowledgments

This study was partly supported by the Japan Society for the Promotion of Science (JSPS), Grant-in-Aid for JSPS Fellows for SO, No. 24-835. We thank T Kogiso (Kyoto University, human and environmental studies) for his help with sample preparation. We also thank Y. Kodama, J. Matsuno, T. Takahashi, and T. Tanabe (Kyoto University, Sci.) for their assistance with our experiments. We appreciate valuable improvements of this manuscript by reviewers, especially by Mario Tribaudino.

References cited

Arlt, T., Kunz, M., Stolz, J., Armbruster, T., and Angel, J.R. (2000) *P-T-X* data on $P2_1/c$-clinopyroxenes and their displacive phase transitions. Contributions to Mineralogy and Petrology, 138, 35-45.

Atlas, L. (1952) The polymorphism of $MgSiO_3$ and solid-state equilibria in the system $MgSiO_3$-$CaMgSi_2O_6$. Journal of Geology, 60, 125-147.

Bowen, N.L. and Schairer, J.F. (1935) The System, MgO-FeO-SiO_2. American Journal of Science [Fifth Series], 29, 151−217.

Carlson, W.D. (1985) Evidence against the stability of orthoenstatite above ~1005 °C at atmospheric pressure in CaO-MgO-SiO_2. Geophysical Research Letters, 12, 409–411.

Carlson, W.D. (1988) Subsolidus phase equilibria on the forsterite-saturated join $Mg_2Si_2O_6$-$CaMgSi_2O_6$ at atmospheric pressure. American Mineralogist, 73, 232–241.

Carlson, W.D., Swinnea, J.S., and Miser, D.E. (1988) Stability of orthoenstatite at high temperature and low pressure. American Mineralogist, 73, 1255–1263.

Christy, A.G. (1995) Isosymmetric structural phase transitions: phenomenology and examples. Acta Crystallographica B, 51, 753–757.

Finkelstein, G. J., Dera, P. K., and Duffy, T. S, (2015) Phase transitions in orthopyroxene (En_{90}) to 49 GPa from single-crystal X-ray diffraction. Physics of the Earth and Planetary Interiors, 244, 78-86.

Foster, W.R. (1951) High-temperature X-ray diffraction study of the polymorphism of $MgSiO_3$. Journal of American Ceramic Society, 34, 255−259.

Foster, W.R. and Lin, H.C. (1975) New data on the forsterite−diopside−silica system. EOS, 56, 470.

Gatta, G.D., Rinaldi, R., Knight, K.S., Molin, G., and Artioli, G. (2007) High temperature structural

and thermoelastic behaviour of mantle orthopyroxene: an in situ neutron powder diffraction study, Physics and Chemistry of Minerals, 34, 185-200.

Huebner, J.S. (1980) Pyroxene phase equilibria at low pressure. Pyroxene: Reviews in Mineralogy (Mineralogical Society of America), 7, 213−288.

Huebner, J.S. and Turnock A.C. (1980) The melting relations at 1 bar of pyroxenesc omposedla rgely of Ca-, Mg-, and Fe-bearing components, American Mineralogist, 65, 225−271.

Ida, T. (2008) Statistical properties of measured X-ray intensities affected by counting loss. Journal of Applied Crystallography, 41, 393-401.

Ida, T., Hibino, H. and Toraya, H. (2003) Devoncolution of instrumental aberrations for synchrotron powder X-ray diffractometry. Journal of Applied Crystallography. 36, 181-187.

Jiang, D., Fujino, K., Tomioka, N., Hosoya, T., and Das, K. (2002) High temperature X-ray difraction study of enstatite up to the melting point. Journal of Mineralogical and Petrological Science, 97, 20-31.

Lindsley, D. H. (1983) Pyroxene thermomeery. American Mineralogist, 68, 477-493.

Lindsley, D. H., and Anderson, D. J. (1983) A two-pyroxene thermometer. Proceedings of the Thirteenth Lunar and Planetary Science Confidence, Part 2. Journal of Geophysical Research, 88, Supplement, A887-A906.

Miyake, A., Shimobayashi, N., and Kitamura, M. (2004) Isosymmetric structural phase transition of orthoenstatite: Molecular dynamics simuration. American Mineralogist, 89, 1667−1672.

Morimoto, N. (1956) The existence of monoclinic pyroxenes with the space group C^5_{2h}-$P2_1/c$. Proceedings of the Japan Academy, 32, 750–752.

Morimoto, N. and Koto, K. (1969) The crystal structure of orthoenstatite. Zeitschrift für Kristallographie, 129, 65–83.

Morimoto, N. and Tokonami, M. (1969) Domain structure of pigeonite and clinoenstatite. American Mineralogist, 54, 725–740.

Nestola, F., and Tribaudino, M. (2003) The structure of *Pbca* orthopyroxenes along the join diopside-enstatite ($CaMgSi_2O_6$-$Mg_2Si_2O_6$). European Journal of Mineralogy, 15, 365–371.

Ohashi, Y. and Finger, L.W. (1973) A possible high-low transition in orthopyroxene and orthoamphiboles. Carnegie Institution of Washington Year Book, 72, 544–547.

Ohi, S., Miyake, A., Shimobayashi, N., Yashima, M., and Kitamura, M. (2008) An isosymmetric phase transition of orthopyroxene found by high-temperature experiment. American Mineralogist, 93, 1682–1685.

Ohi, S., Miyake, A., and M, Yashima (2010) Stability field of the high-temperature orthorhombic phase in the enstatite-diopside system. American Mineralogist, 95, 1267–1275.

Pannhorst, W. (1979) Structural relationships between pyroxenes. Neues Jahrbuch für Mineralogie Abhandlungen, 135, 1–17.

Smith, J.V. (1969) Magnesium pyroxenes at high temperature: Inversion in clinoenstatite. Nature, 222, 256–257.

Smyth J. R., and Burnham C. W. (1972) The crystal structures of high and low clinohypersthene. Earth and Planetary Science Letters, 14, 183-189.

Toraya, H., Huang, H. C., and Wu, Y. (1993) Intensity enhancement in asymmetric diffraction with parallel-beam synchrotron radiation. Journal of Applied Crystallography. 26, 774-777.

Toraya, H., Hibino, H., and Ohsumi, K. (1996) A new powder diffractometer for synchrotron radiation with a multiple-detector system. Journal of Synchrotron Radiation, 3, 75–83.

Tribaudino, M., and Nestola, F. (2002) Average and local structure in $P2_1/c$ clinopyroxenes along the join diopside-enstatite ($CaMgSi_2O_6$-$Mg_2Si_2O_6$). European Journal of Mineralogy, 14, 549–555.

Tribaudino, M., Nestola, F., Cámara, F., and Domeneghetti, M. C. (2002) The high-temperature

$P2_1/c$-$C2/c$ phase transition in Fe-free pyroxene ($Ca_{0.15}Mg_{1.85}Si_2O_6$): Structural and thermodynamic behavior. American Mineralogist, 87, 648-657.

Tsuchiyama, A., Fujita, T., and Morimoto, N. (1988) Fe-Mg homogenization of pyroxene in the low-Ca pyroxene during metamorphism of the ordinary chondrites. Proceedings of the NIPR Symposium on Antarctic Meteorites. 1 ,173-184.

Turnock, A. C., and Lindsly, D. H. (1981) Experimental determination of pyroxene solvi for ≤ 1 kbar at 900 and 1000 °C. Canadian Mineralogist, 19, 255-267.

Yanai, K. and Kojima, H. (1995) Yamato-8451: A new identified pyroxene-bearing pallasite, Proceedings of the NIPR Symposium on Antarctic Meteorites. 8,1-10.

Yang, H. and Ghose, S. (1994) In-situ Fe-Mg order-disorder studies and thermodynamic properties of orthopyroxene $(Mg,Fe)_2Si_2O_6$. American Mineralogist, 79, 633–643.

Yang, H. and Ghose, S. (1995) A transitional structural state and anomalous Fe–Mg order–disorderin Mg-rich orthopyroxene, $(Mg_{0.75}Fe_{0.25})_2Si_2O_6$. American Mineralogist, 80, 9–20.

Yang, H., Finger, L.W., Conrad, P. G., Prewitt, C. T., and Hazen, R. M. (1999) High-pressure single-crystal X-ray diffraction and Raman study of the *Pbcn*-$P2_1cn$ phase transition in protopyroxene. American Mineralogist, 84, 245-256.

Zhang, J. S., Dera, P., and Bass, J. D. (2012) A new high-pressure phase transition in natural Fe-bearing orthoenstatite. American Mineralogist, 97, 1070-1074.

Figure 1. Schematic phase diagram for the $Mg_2Si_2O_6$(En)-$Fe_2Si_2O_6$(Fs) system at 1 atm after Huebner (1980). Ppx = protopyroxene; Opx = orthopyroxene; Pig = pigeonite; Ol = olivine; L = liquid.

Figure 2. Sample assemblage for synthesis of $Fs_{20}S$.

Figure 3. High-temperature X-ray powder diffraction patterns at various temperatures for natural and synthetic Opx samples with magnified views around the 610 diffraction peak. (a) to (f) Natural Opx samples (Fs_{10}, Fs_{14}, and Fs_{37}) and (g) to (l) synthetic Opx (Fs_{20}, Fs_{30}, and Fs_{46}). Diffraction peaks are labeled with Miller indices; those annotated L and H are for low- and high-temperature Opx, respectively. Ol = olivine, HT-Cpx = high-temperature clinopyroxene (high-temperature pigeonite), Qtz = quartz. Numbers appended diffraction patterns indicate temperatures (°C).

Figure 4. Unit cell dimensions (*a*, *b*, and *c*) and volume (*V*) of Opx samples versus temperature. Error bars shown are almost the same size as the symbols. (a) to (c) Natural Opx, (d) to (f) synthetic Opx.

Figure 5. Schematic phase diagram of the $Mg_2Si_2O_6$(En)-$Fe_2Si_2O_6$(Fs) system showing stability fields of LT-Opx and HT-Opx and transitions from LT-Opx to HT-Opx observed in this and previous studies. Thick solid and dashed lines indicate transition temperatures for synthetic and natural Opx, respectively, according to this study. Thin solid lines mark phase boundaries according to previous studies. Thin dashed lines mark phase boundaries according to this study.

Table 1. Chemical compositions of orthopyroxenes in starting samples and locations of sources of natural orthopyroxenes.

Table 2. Unit cell dimensions and volumes of Opx at room and high temperatures.

Figure 1

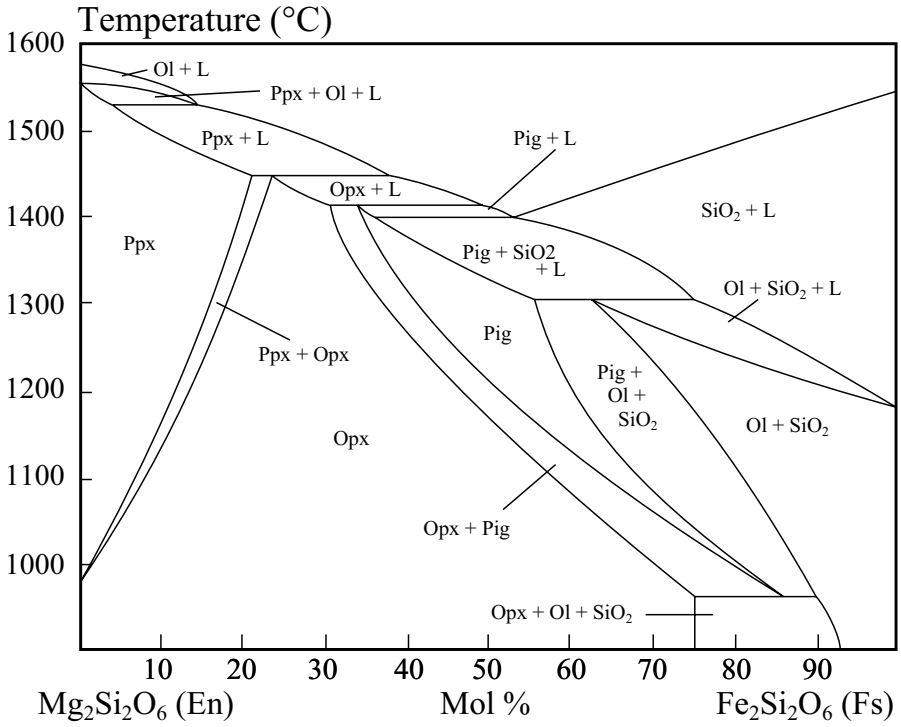
Temperature (°C)
1600
1500
1400
1300
1200
1100
1000
Ol + L
Ppx + Ol + L
Ppx + L
Pig + L
Opx + L
SiO2 + L
Ppx
Pig + SiO2 + L
Ol + SiO2 + L
Pig
Ppx + Opx
Pig + Ol + SiO2
Ol + SiO2
Opx
Opx + Pig
Opx + Ol + SiO2
10
20
30
40
50
60
70
80
90
Mg2Si2O6 (En)
Mol %
Fe2Si2O6 (Fs)

Figure 2

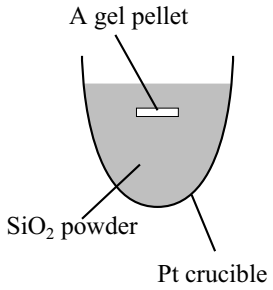

Figure 3_1

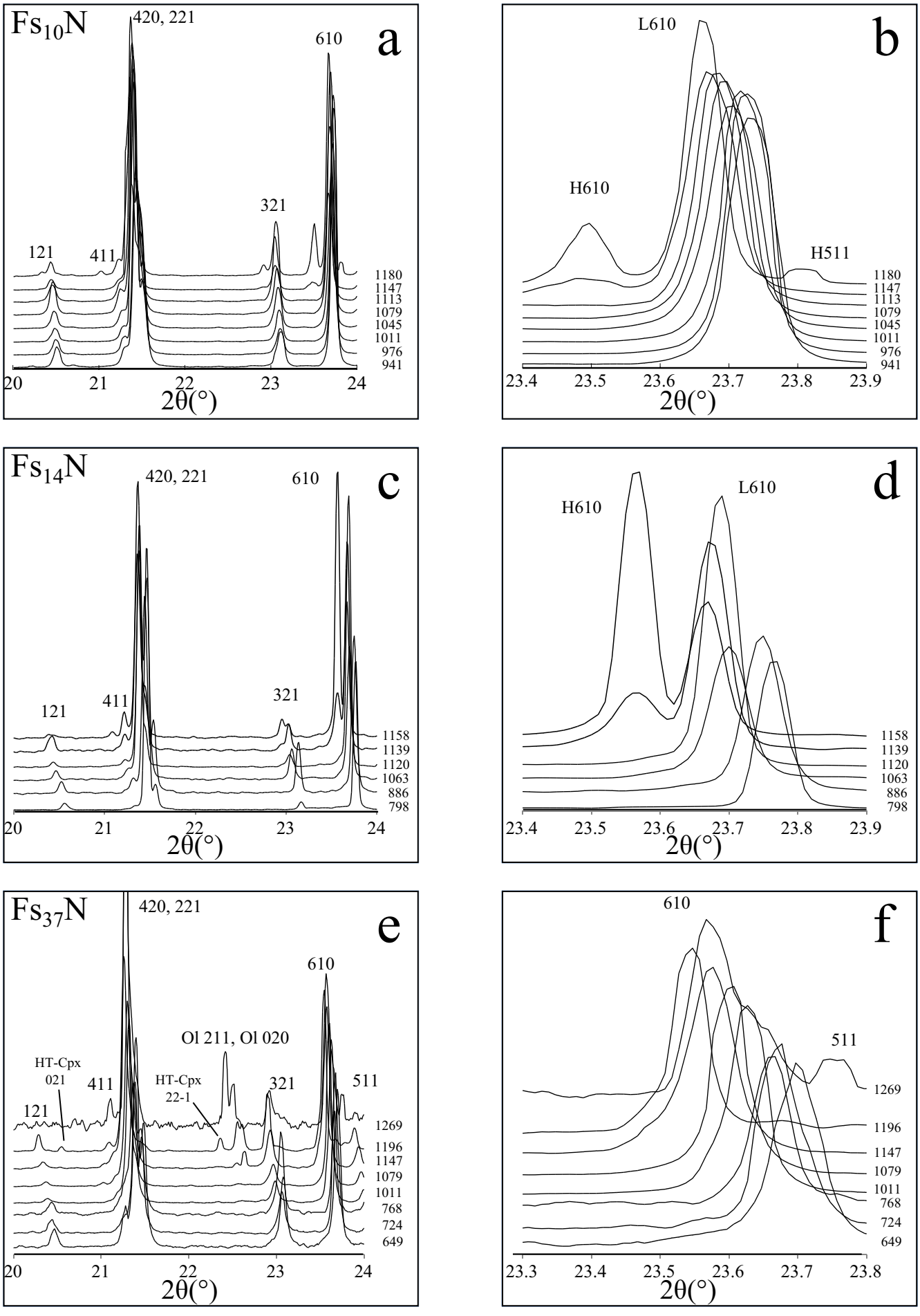
Fs10N
420, 221
610
a
121
411
321
1180
1147
1113
1079
1045
1011
976
941
20
21
22
23
24
2θ(°)
L610
b
H610
H511
23.4
23.5
23.6
23.7
23.8
23.9
Fs14N
c
1158
1139
1120
1063
886
798
d
Fs37N
e
Ol 211, Ol 020
HT-Cpx
021
HT-Cpx
22-1
511
1269
1196
768
724
649
f

Figure 3_2

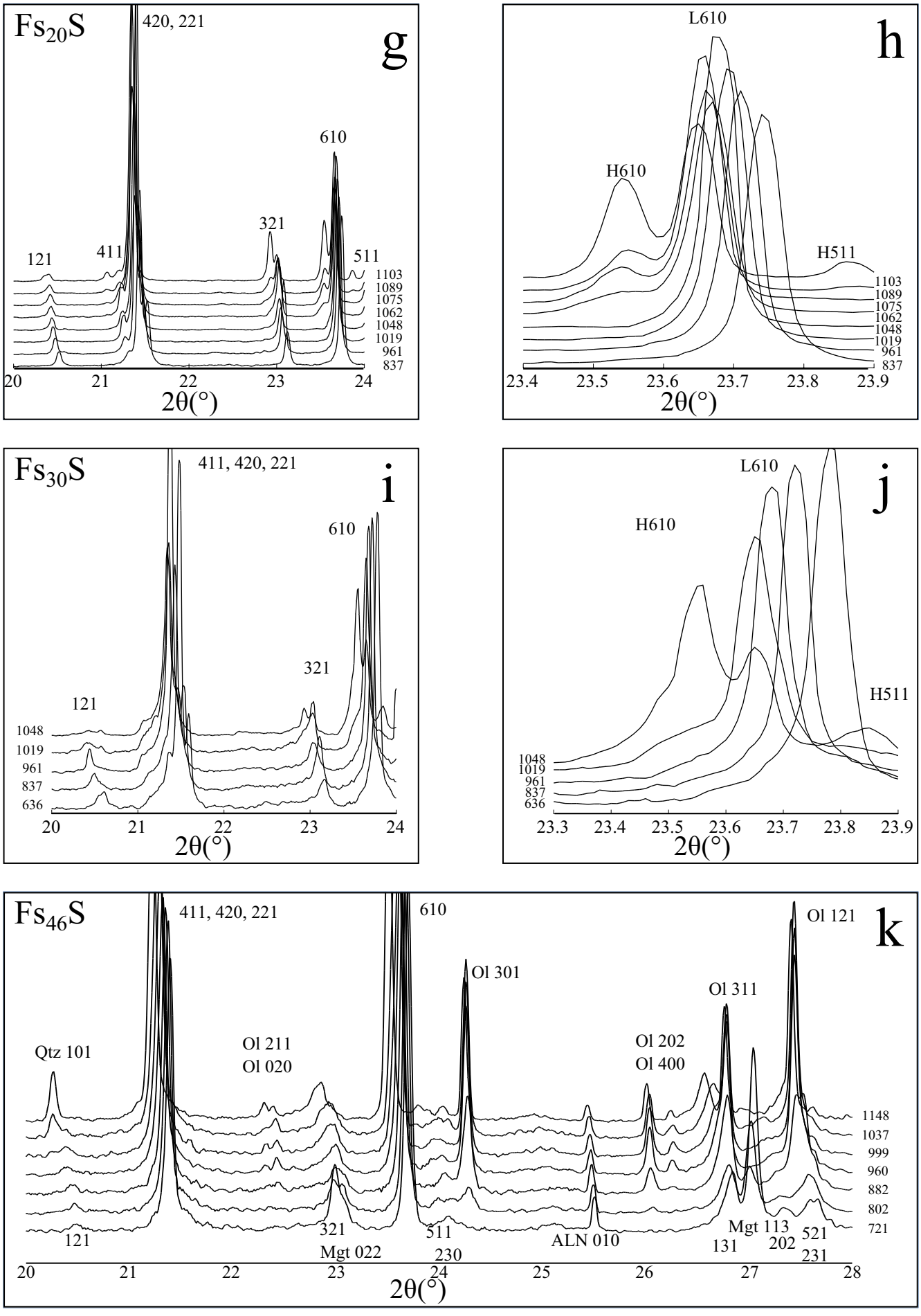
Fs20S
420, 221
g
610
321
121
411
511
1103
1089
1075
1062
1048
1019
961
837
20
21
22
23
24
2θ(°)
L610
h
H610
H511
23.4
23.5
23.6
23.7
23.8
23.9
Fs30S
411, 420, 221
i
610
321
121
1048
1019
961
837
636
j
L610
H610
H511
23.3
Fs46S
411, 420, 221
610
Ol 121
k
Ol 301
Ol 311
Qtz 101
Ol 211
Ol 020
Ol 202
Ol 400
1148
1037
999
960
882
802
721
321
511
Mgt 022
230
ALN 010
Mgt 113
131
202
521
231
25
26
27
28

Figure 3_3

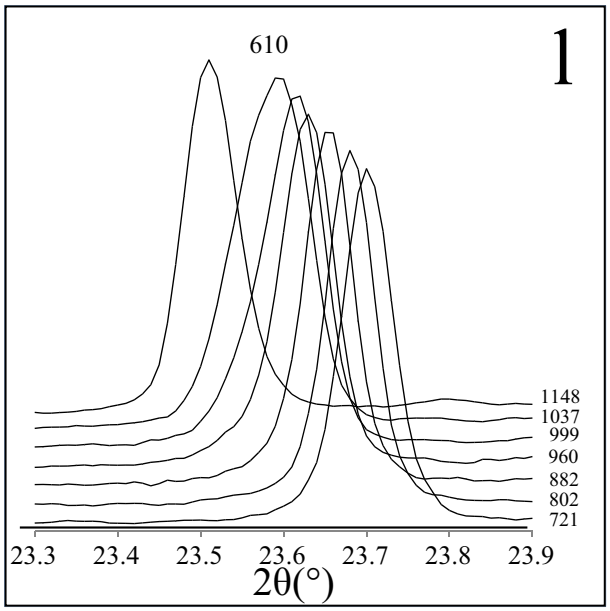
610
1
1148
1037
999
960
882
802
721
23.3
23.4
23.5
23.6
23.7
23.8
23.9
2θ(°)

Figure 4

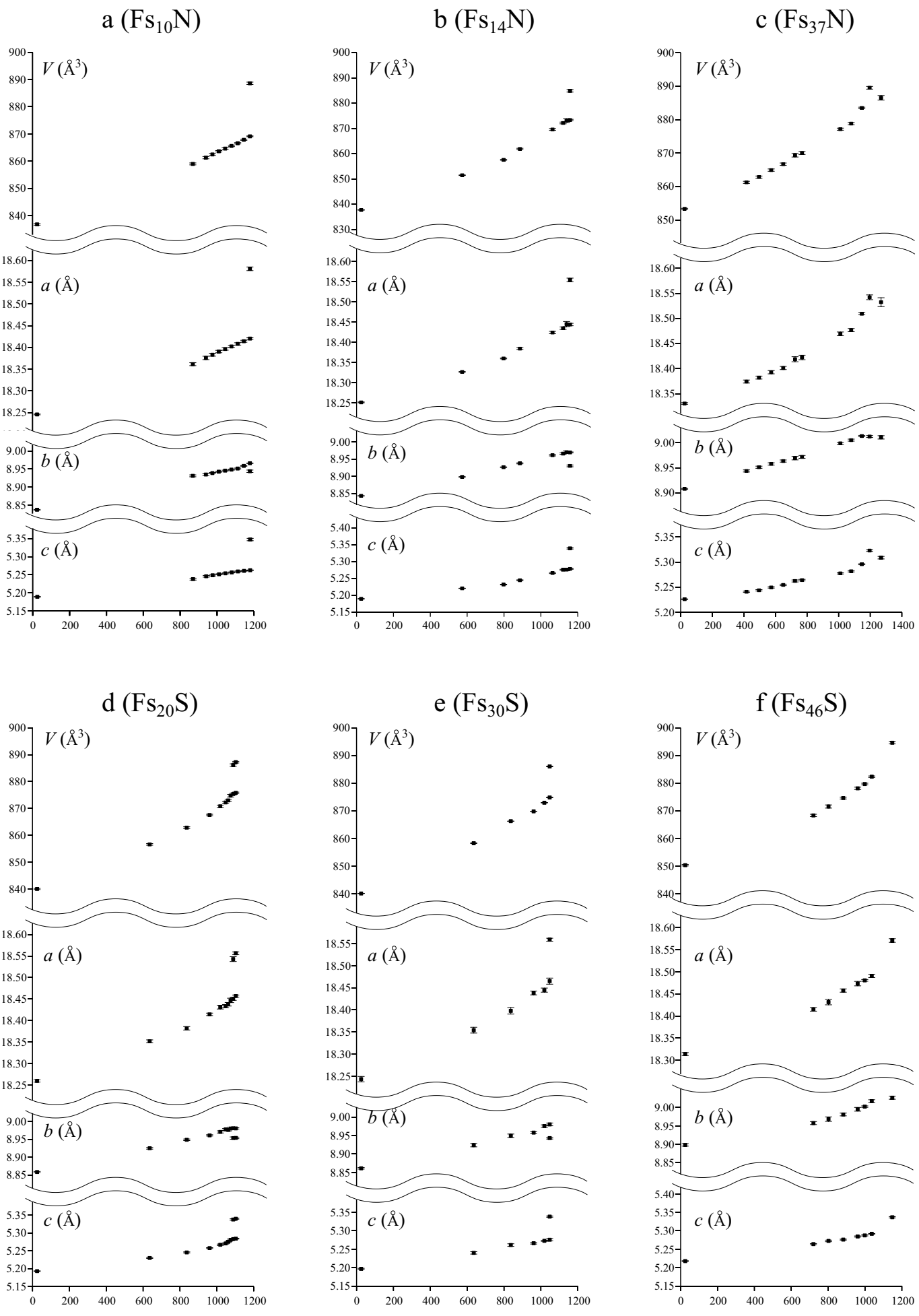

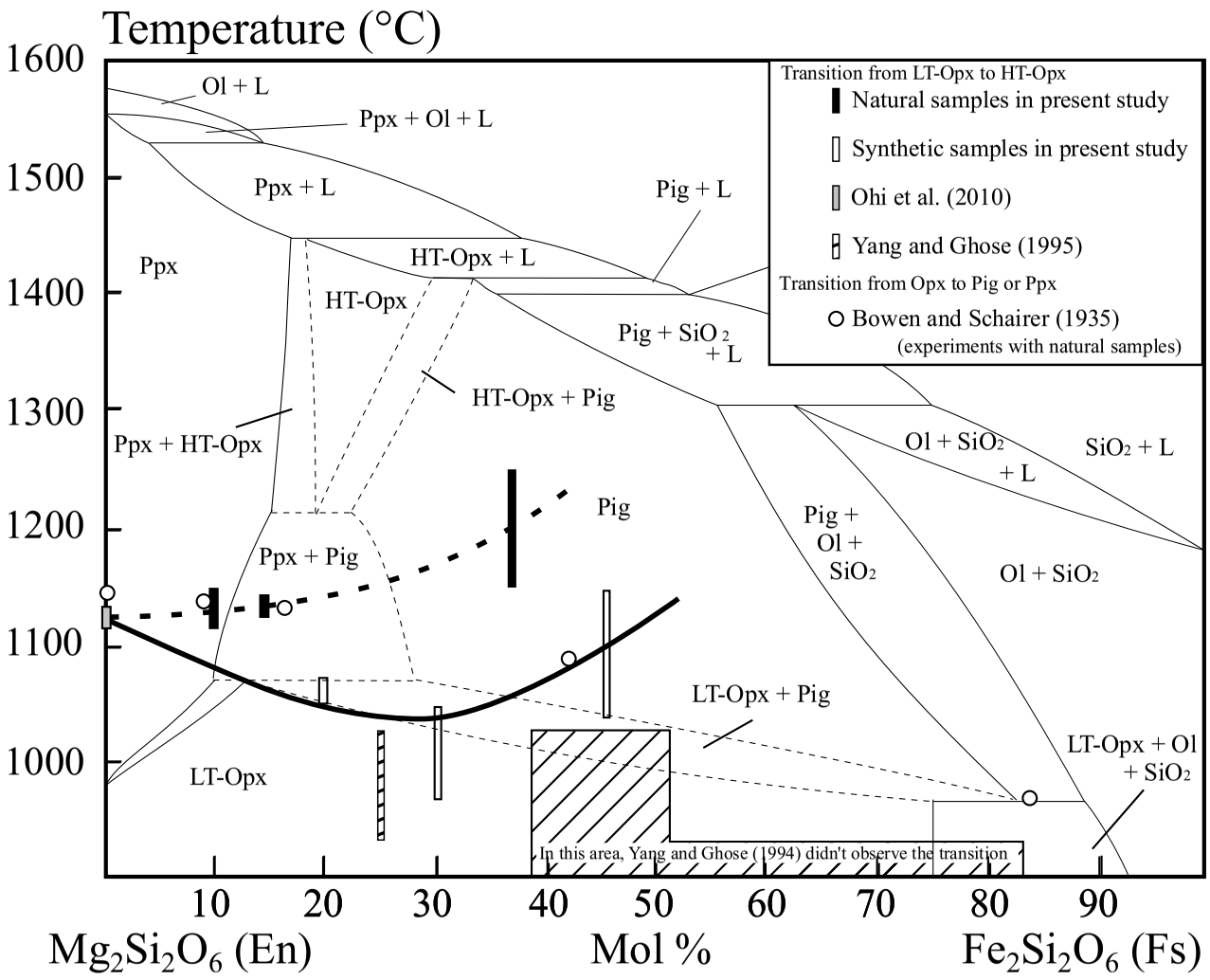
Temperature (°C)
1600
1500
1400
1300
1200
1100
1000
Ol + L
Ppx + Ol + L
Ppx + L
Pig + L
Ppx
HT-Opx + L
HT-Opx
Pig + SiO 2
+ L
HT-Opx + Pig
Ppx + HT-Opx
Ol + SiO2
+ L
SiO2 + L
Pig
Pig +
Ol +
SiO2
Ol + SiO2
Ppx + Pig
LT-Opx + Pig
LT-Opx + Ol
+ SiO2
LT-Opx
In this area, Yang and Ghose (1994) didn't observe the transition
Transition from LT-Opx to HT-Opx
Natural samples in present study
Synthetic samples in present study
Ohi et al. (2010)
Yang and Ghose (1995)
Transition from Opx to Pig or Ppx
Bowen and Schairer (1935)
(experiments with natural samples)
10
20
30
40
50
60
70
80
90
Mg2Si2O6 (En)
Mol %
Fe2Si2O6 (Fs)

	Na	Mg	Al	Si	Ca	Ti	Cr	Mn	Fe	O	locality
$Fs_{10}N$	0.02	1.83	0.02	1.98	0.01	ND	ND	0.00	0.19	6.00	Morogoro, Tanzania
$Fs_{14}N$	0.02	1.70	0.00	2.01	0.01	ND	ND	0.00	0.27	6.00	Bamble, Norway
$Fs_{37}N$	ND	1.19	0.02	2.01	0.03	ND	ND	0.03	0.69	6.00	Ibaragi, Japan
$Fs_{20}S$	-	1.57	-	2.02	-	-	-	-	0.40	6.00	synthetic
$Fs_{30}S$	-	1.35	-	2.03	-	-	-	-	0.59	6.00	synthetic
$Fs_{46}S$	-	1.11	-	1.99	-	-	-	-	0.91	6.00	synthetic

Fs10N	T (°C)		a (Å)	b (Å)	c (Å)	V (Å^3)
	25		18.245(1)	8.837(1)	5.189(1)	836.7(1)
	870		18.361(3)	8.931(2)	5.238(1)	859.0(4)
	941		18.376(4)	8.935(2)	5.246(2)	861.3(4)
	976		18.383(3)	8.939(2)	5.249(2)	862.4(4)
	1011		18.390(3)	8.943(1)	5.251(1)	863.6(3)
	1045		18.396(3)	8.946(1)	5.254(1)	864.6(3)
	1079		18.402(3)	8.948(1)	5.256(1)	865.6(3)
	1113		18.408(3)	8.951(1)	5.259(1)	866.6(2)
	1147		18.414(2)	8.959(1)	5.261(1)	867.8(2)
	1180	LT-Opx	18.420(2)	8.966(1)	5.262(1)	869.1(1)
		HT-Opx	18.580(4)	8.944(3)	5.347(1)	888.6(4)

Fs20S	T (°C)		a (Å)	b (Å)	c (Å)	V (Å^3)
	25		18.260(3)	8.859(2)	5.193(1)	840.0(2)
	636		18.352(3)	8.925(2)	5.230(1)	856.6(3)
	837		18.382(4)	8.949(2)	5.245(2)	862.8(3)
	961		18.414(3)	8.961(2)	5.258(1)	867.6(3)
	1019		18.431(4)	8.971(3)	5.267(2)	870.8(4)
	1048		18.434(4)	8.978(3)	5.270(2)	872.2(4)
	1062		18.438(4)	8.976(3)	5.275(2)	873.0(4)
	1075		18.447(5)	8.980(3)	5.280(2)	874.7(5)
	1089	LT-Opx	18.451(3)	8.981(3)	5.283(2)	875.4(4)
		HT-Opx	18.543(6)	8.954(3)	5.337(2)	886.1(5)
	1103	LT-Opx	18.457(2)	8.981(2)	5.284(1)	875.8(2)
		HT-Opx	18.557(3)	8.954(2)	5.340(1)	887.2(3)

Fs14N	T (°C)		a (Å)	b (Å)	c (Å)	V (Å^3)
	25		18.251(1)	8.8432(6)	5.1900(3)	837.68(9)
	573		18.327(1)	8.8985(8)	5.2210(4)	851.4(1)
	798		18.360(1)	8.9269(8)	5.2322(6)	857.5(1)
	886		18.384(2)	8.938(1)	5.245(1)	861.9(3)
	1063		18.424(3)	8.962(2)	5.267(2)	869.6(4)
	1121		18.435(3)	8.966(2)	5.276(1)	872.2(3)
	1139		18.445(6)	8.971(3)	5.277(3)	873.1(8)
	1158	LT-Opx	18.444(3)	8.970(1)	5.279(1)	873.3(3)
		HT-Opx	18.554(4)	8.931(2)	5.340(2)	884.9(5)

Fs30S	T (°C)		a (Å)	b (Å)	c (Å)	V (Å^3)
	25		18.243(6)	8.860(2)	5.197(1)	840.0(4)
	636		18.354(7)	8.924(5)	5.240(3)	858.2(8)
	837		18.398(7)	8.949(5)	5.261(3)	866.2(8)
	961		18.438(4)	8.958(3)	5.266(2)	869.8(5)
	1019		18.445(5)	8.976(3)	5.273(1)	872.9(4)
	1048	LT-Opx	18.465(7)	8.980(4)	5.276(3)	874.8(7)
		HT-Opx	18.559(3)	8.943(2)	5.338(2)	886.0(4)

Fs37N	T (°C)	a (Å)	b (Å)	c (Å)	V (Å^3)
	25	18.331(2)	8.908(1)	5.2262(6)	853.4(2)
	417	18.375(3)	8.944(2)	5.241(1)	861.3(3)
	496	18.382(3)	8.951(2)	5.244(1)	862.9(3)
	572	18.393(3)	8.958(2)	5.250(1)	864.9(3)
	649	18.401(3)	8.964(2)	5.255(2)	866.7(4)
	724	18.419(5)	8.969(3)	5.262(2)	869.4(5)
	768	18.422(4)	8.972(3)	5.264(2)	870.1(4)
	1011	18.470(4)	8.999(2)	5.278(1)	877.2(3)
	1079	18.477(3)	9.005(2)	5.282(1)	878.8(3)
	1147	18.509(2)	9.013(1)	5.296(1)	883.5(2)
	1196	18.542(5)	9.012(2)	5.323(2)	889.5(4)
	1269	18.533(9)	9.010(3)	5.309(3)	886.5(7)

Fs46S	T (°C)	a (Å)	b (Å)	c (Å)	V (Å^3)
	25	18.314(3)	8.898(1)	5.218(1)	850.3(3)
	721	18.415(4)	8.958(3)	5.264(2)	868.3(4)
	802	18.431(6)	8.968(4)	5.272(2)	871.5(6)
	882	18.457(4)	8.981(2)	5.276(1)	874.6(3)
	961	18.473(5)	8.995(2)	5.284(2)	878.1(4)
	999	18.480(2)	9.002(1)	5.287(1)	879.6(3)
	1037	18.491(4)	9.017(1)	5.292(1)	882.3(3)
	1148	18.570(4)	9.026(2)	5.337(2)	894.6(4)